

Bubble dynamics in a Hele-Shaw cell: Exact solutions and the dynamical mechanism for velocity selection

Giovani L. Vasconcelos*

*Departamento de Física, Universidade Federal do Paraná,
81531-990 Curitiba, Paraná, Brazil*

Arthur A. Brum

*Departamento de Física,
Universidade Federal de Pernambuco,
50670-901, Recife, Brazil*

Mark Mineev-Weinstein†

New Mexico Consortium, Los Alamos, NM, 87544, USA;

Abstract

The unsteady motion of a bubble in a Hele-Shaw channel is analyzed in the case when surface tension is neglected.

PACS numbers: 47.20.Hw, 47.20.Ma, 47.15.km, 02.30.Ik

*Electronic address: giovani.vasconcelos@ufpr.br

†Electronic address: mark_mw@hotmail.com

I. INTRODUCTION

The motion of the interface between two fluids in a Hele-Shaw cell—a system where the fluids are confined between two closely spaced glass plates—has attracted considerably attention in both the physics and mathematics literature since the pioneering work of Saffman and Taylor [1, 2]. On the one hand, the Hele-Shaw model [3] is analogous to several other physical systems, such as flows in porous media [4, 5], dendritic solidification [6], combustion fronts [7], electromigration of voids [8], streamer ionization fronts [9], and bacterial colony growth [10], which are all governed (under certain approximations) by similar equations of motion [11]. On the other hand, Hele-Shaw flows have deep mathematical connections with several apparently unrelated problems in mathematical physics, such as 2D quantum gravity [12], integrable systems [13], random matrix [14], quantum hall effect [15], and Loewner evolution [16]. As a result, Hele-Shaw flows have become a fertile laboratory to study interface dynamics, pattern formation, and other related problems.

The Hele-Shaw system is particularly interesting when one of the fluids is much less viscous than the other and surface tension effects are neglected. In this case, the problem becomes quite tractable mathematically and many exact solutions have been found, since the solutions obtained by Saffman and Taylor for a steadily moving finger [1] or bubble [2]. A rather complete set of steady solutions for fingers and bubbles has been described in Ref. [17], where a brief review of earlier solutions is also given. Time dependent solutions are more difficult to obtain, but starting with the solution for a finger growing from a flat interface obtained by Saffman [18], several exact solutions have been found both for the growth of fingers in a channel [19, 20] and for an expanding bubble in an unbounded cell [19, 21, 22]. Exact time-dependent solutions for multiply connected geometries have also been obtained both in an unbounded cell [23–27] and in the channel geometry [28–30], including the problem of Hele-Shaw flows past obstacles [31, 32].

One particular aspect of the Hele-Shaw interface dynamics that has attracted a great deal of attention is the so-called *selection problem*, first posited by Saffman and Taylor [1] in the context of viscous fingering. It concerns the question as to why the finger reaches a relative width $\lambda = 1/2$, implying that the finger velocity U is *twice* the velocity V of the background fluid, i.e, $U = 2V$, despite the fact the problem admits a continuum of exact solutions with $0 < \lambda < 1$. In the mid 1980s, it was shown by several groups [33] through a beyond-all-

orders asymptotic analysis that the inclusion of surface tension leads to a countable infinity of steady solutions, all of which converge to $U = 2V$ when the surface tension parameter is taken to zero. Similar analysis was performed for the case of a single bubble in a Hele-Shaw channel [34, 35], where the velocity $U = 2V$ was again selected. It was subsequently found that other boundary conditions, such as kinetic undercooling [36, 37], also lead to the same selection scenario. More strikingly, similar pattern selection has also been observed in non-fluid systems, such as finger-like ionization fronts in electric breakdown [9], where there is no analog of surface tension. The effect of surface tension on one and two bubbles in an unbounded cell [38] was also studied and the same selected velocity $U = 2V$ was obtained.

The results above show that velocity selection in a Hele-Shaw cell is not particularly dependent on the boundary condition (or lack thereof) that one chooses to ‘regularize’ the idealized problem, as the same velocity $U = 2V$ is always obtained. Indeed, it has been known since the late 1990’s that the finger selection problem can be addressed entirely within the context of time-dependent solutions *without surface tension*. More specifically, it was shown [39] that in this case the steady solution with $\lambda = 1/2$ is the only stable attractor of the dynamics. Recently two of the present authors [40] reported an exact time-dependent solution for a single bubble evolving in a Hele-Shaw channel, from which it was possibly to show that the velocity $U = 2V$ is again the only stable attractor. Similar result was subsequently obtained for a bubble in an unbounded Hele-Shaw cell [41], where it was found that the circle (which has $U = 2V$) is the only stable solution. More recently, it has been shown that the same selection mechanism (without surface tension) holds for any number of bubbles in a Hele-Shaw channel [42].

In this paper we consider the problem of the unsteady motion of a single bubble in a Hele-Shaw channel in the absence of surface tension. Here we discuss in greater detail the general class of time-dependent exact previously reported in condensed form in Ref. [40]. Our solutions are constructed as a conformal mapping from a doubly-connected circular domain in an auxiliary complex ζ -plane to the fluid region exterior to the bubble in the physical z -plane. The corresponding mapping function $z(\zeta, t)$, where t denotes time, possesses only logarithmic singularities and is given explicitly in terms of certain special functions (related to the Jacobi theta functions).

The motion of the singularities in the ζ -plane is determined by a set of conserved quantities, which in turn are related to the *fixed singularities* of the Schwarz function $S(z, t)$ of

the bubble interface; see below for a definition of $S(z, t)$. The existence of such conservation laws is a manifestation of the integrable nature of the problem of interface dynamics in a Hele-Shaw cell, also known as Laplacian growth [12]. The infinite-dimensional problem of interface motion in a Hele-Shaw cell is thus reduced to a dynamical system, sometimes referred to as “pole dynamics” [22], corresponding to the motion of a finite number of singularities of the mapping $z(\zeta, t)$. Here we show that this dynamical system for the case of a bubble in a channel has only two fixed points in the ζ -plane, one stable and the other unstable, which correspond to simple poles of $S(z, t)$ at the channel endpoints $x = -\infty$ and $x = +\infty$, respectively.

We show furthermore that that under generic initial conditions the bubble will approach a steady regime with velocity $U = 2V$. To obtain bubbles traveling with velocity $U \neq 2V$ one must start, in contradistinction, from a restricted set of initial conditions—namely, those having singularities at precisely the fixed points, but since one the fixed point is unstable any perturbation from such an initial shape (i.e., that displaces the singularity from the unstable fixed point) will result in a steady shape with $U = 2V$. In other words, the steady solutions where the bubble moves twice as fast as the background fluid are generally selected, as they are the only stable attractor of the dynamics, in agreement with the previous results mentioned above [39, 40]. Seen from the perspective of the Schwarz function of the interface, these results mean that $S(z, t)$ is *regular* at infinity for all initial conditions leading to the asymptotic velocity $U = 2V$, whereas it has a simple pole at infinity for non-generic initial conditions that result in $U \neq 2V$ (but any perturbation ‘displacing’ this singularity from infinity will lead instead to $U = 2V$, as just mentioned).

The selection scenario described above is akin to the dynamical mechanism for velocity selection [43, 44] observed in systems possessing traveling-wave solutions with different velocities, where most of the “natural” initial conditions lead to the same asymptotic velocity. More specifically, initial conditions that decay sufficiently rapidly at infinity lead to profiles that asymptotically spread with the same velocity [45]. Similarly, in our case, the behavior of the initial conditions at infinity also determine the asymptotic velocity, as discussed in the preceding paragraph.

As already mentioned, the degeneracy of the interface velocity may also be lifted by the inclusion of some singular effect (say, surface tension) that is neglected in the idealized model. Nonetheless, the dynamical selection criterion is important to establish which are the

solutions that “survive” the singular perturbation [43] and also to explain why the system is dynamically driven to the selected pattern. In this sense, one may argue that solving the selection problem (at least in the context of Hele-Shaw flows) does not necessarily require the inclusion of regularizing boundary conditions, as the problem can be dynamically addressed entirely within the context of the idealized system. Specific details of the selected physical shape, such as the pattern symmetry, might of course depend on surface tension. Indeed, our framework does not, so far, preclude non-symmetric steady shapes, whereas only symmetric bubbles seem to survive the inclusion of surface tension [34]. Velocity selection, however, does not require surface tension, as it has an underlying dynamical origin, as argued above and shown in more detail later.

Furthermore, the dynamical mechanism also helps to explain why selection does *not* take place in certain situations, even after the inclusion of surface tension. One such instance is the case of a periodic array of Hele-Shaw bubbles, where no velocity selection is observed when one considers surface tension effects [46]. The lack of selection in this case can be nicely understood within the scope of the selection scenario outlined above. The important point to note here is that the Schwarz function of the steady periodic solutions [17] is free from singularity in the fluid domain (i.e., in a period cell) for any value of U , contrarily to the case of a single steady bubble (or a finite number of them [42]), where only for $U = 2V$ is the Schwarz function regular in the entire fluid region. As there is no preferred velocity in the periodic geometry, the observed velocity will depend on the size and separation of the bubbles, which is precisely the result obtained in Ref. [46].

The present paper is organized as follows. In Sec. II we formulate the problem of the unsteady motion of a bubble in a Hele-Shaw channel. An exact solution in terms of a conformal mapping from a doubly-connected circular domain to the fluid region exterior to the bubble is presented in Sec. III, and several numerical examples of time-evolving bubbles are shown in Sec. IV. In Sec. V we present a stability analysis that shows that the steady solutions with $U = 2V$ ($U \neq 2V$) are attractors (repellers) of the dynamics. Our main findings and conclusions are summarized in Sec. VI.

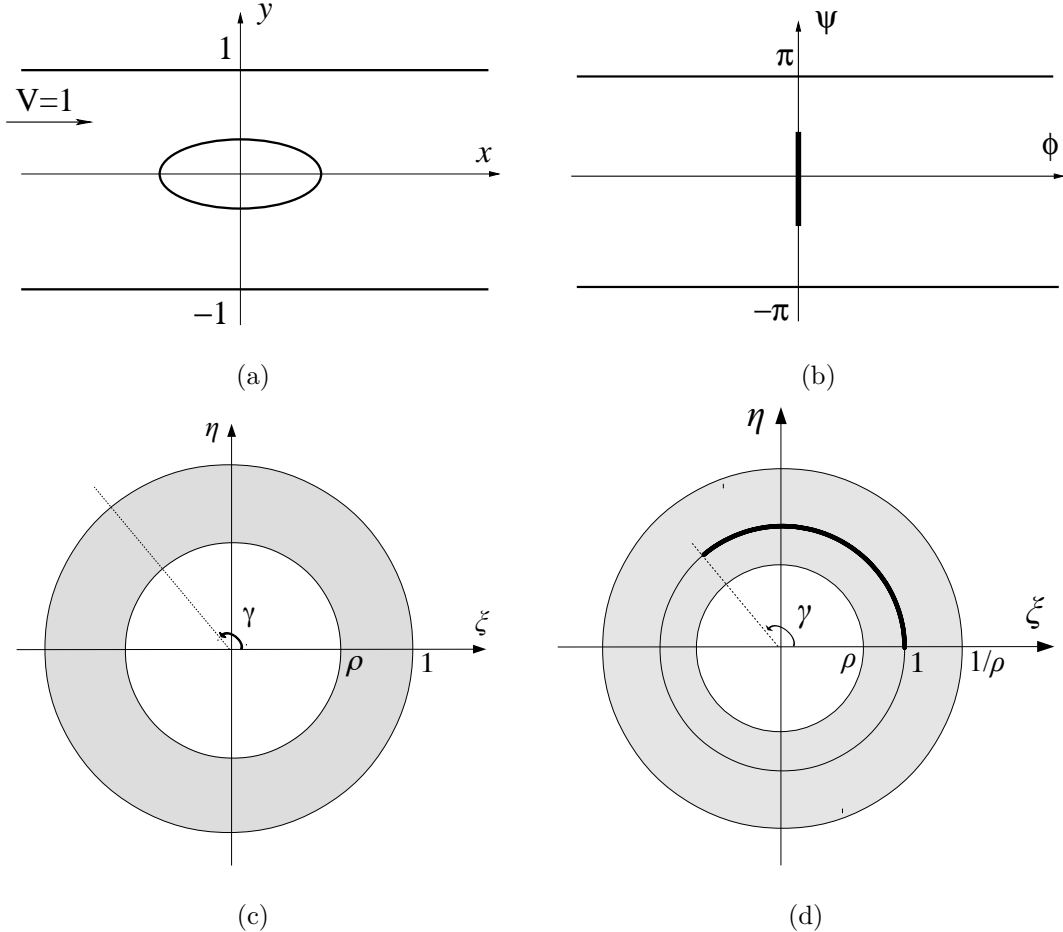


Figure 1: The flow domains for a single bubble in a Hele-Shaw channel: (a) the physical z -plane; (b) the plane of the complex potential; (c) the auxiliary complex ζ -plane; and (d) the extended domain in the ζ -plane.

II. FORMULATION OF THE PROBLEM

We consider the problem of a single bubble of a less viscous fluid (say, air) moving in a more viscous fluid (say, oil) inside a Hele-Shaw channel, which consists two parallel rectangular glass plates separated by a small gap b . The viscous fluid domain (outside the bubble) is denoted by $D(t)$, while the bubble boundary is denoted by ∂D_t . The fluid inside the bubble is considered to be inviscid and is assumed to be at a constant pressure $p_0 = 0$. The viscous fluid is injected at a uniform rate by a source located at $x = -\infty$ and removed by a sink located at $x = +\infty$, thus generating a uniform flow with velocity V in the far-field from the interface. Here we choose for convenience the channel width to be π and set the far-field velocity to unity, i.e., $V = 1$; see Fig. 1(a) for a schematics of the flow geometry.

Under the usual approximations [11], the dynamics in a Hele-Shaw cell is governed by Darcy's law, $\mathbf{v} = -\frac{b^2}{12\mu}\nabla p$, where $\mathbf{v}(x, y, t)$ is the velocity vector field, $p(x, y, t)$ is the pressure field, b is the cell gap, and μ is the fluid viscosity. Hele-Shaw flows are thus potential flows, i.e., $\mathbf{v} = \nabla\phi$, where the velocity potential is $\phi = -\frac{b^2}{12\mu}p$. Assuming that the viscous fluid is incompressible, $\nabla \cdot \mathbf{v} = 0$, we find that ϕ obeys the 2D Laplace equation, $\nabla^2\phi = 0$. Because of the uniform flow at infinity we have $\phi = x$ for $x \rightarrow \pm\infty$. Also, $\partial_n\phi = 0$ (no normal flow) at both boundaries of the channel at $y = 0$ and $y = \pi$, where ∂_n denotes the normal derivative. Furthermore, we shall neglect surface tension effects so that $p = 0$ along the moving interface ∂D_t , which implies that $\phi = 0$ on ∂D_t . Finally, the kinematic boundary condition requires that the normal velocities of the moving boundary, V_n , and of the viscous fluid, v_n , coincide, so $V_n = \partial_n\phi$ at the moving interface ∂D_t . The full mathematical formulation of the problem thus takes the following form:

$$\nabla^2\phi = 0 \quad \text{in} \quad D_t, \quad (1a)$$

$$\phi = 0 \quad \text{at} \quad \partial D_t, \quad (1b)$$

$$V_n = -\partial_n\phi \quad \text{at} \quad \partial D_t, \quad (1c)$$

$$\phi = x \quad \text{for} \quad x \rightarrow \pm\infty, \quad (1d)$$

$$\partial_n\phi = 0 \quad \text{at} \quad y = 0 \text{ and } y = \pi. \quad (1e)$$

In the next section we shall reformulate the problem in terms of a conformal mapping map from a circular domain in an auxiliary complex plane to the physical plane.

A. The conformal mapping

We seek a solution to the problem in the form of a conformal map $z(\zeta, t)$ from a circular domain D_ζ in an auxiliary complex ζ -plane to the fluid region D_z in the z -plane. The domain D_ζ consists of an annulus comprehended between the unit circle C_0 and an inner circle C_1 of radius ρ ; see Fig. 1(c). The inner circle C_1 is chosen to map to the interface (bubble boundary); while the unit circle C_0 maps to the channel walls, with the point $\zeta_+ = 1$ mapping to $x = \infty$ and the point $\zeta_- = e^{i\gamma}$, $0 < \gamma < 2\pi$, mapping to $x = -\infty$. The mapping function $z(\zeta, t)$ must thus have logarithmic singularities at $\zeta = \zeta_\pm$:

$$z(\zeta, t) \approx \mp \ln(\zeta \mp \zeta_\pm), \quad \text{for} \quad \zeta \rightarrow \zeta_\pm. \quad (2)$$

It is convenient to consider an augmented flow domain in the z -plane consisting of the original channel plus its reflection in the real axis, so that there are now two bubbles within the flow domain which are the mirror reflection of one another with respect to the centreline (real axis) of the extended channel — in such extended domain the solution is periodic in the y direction with period 2π . The extended domain in the ζ -plane, to be denoted by F_0 , is obtained by adding to D_ζ its reflection in the unit circle C_0 , thus generating an extended annulus:

$$F_0 = D_\zeta \cup \varphi_0(D_\zeta) = \{\zeta \mid \rho < |\zeta| < 1/\rho\}, \quad (3)$$

as shown in Fig. 1(d). The function $z(\zeta, t)$ thus maps F_0 to the extended channel in the z -plane defined above.

B. The complex potential

As the velocity potential $\phi(x, y, t)$ is a harmonic function, it is convenient to introduce the complex potential $w(z, t) = \phi(x, y, t) + i\psi(x, y, t)$, where $z = x + iy$ and $\psi(x, y, t)$ is the stream function. It then follows from (1) that the complex potential $w(z, t)$ must be analytic in $D(t)$ and satisfy the following boundary conditions:

$$w(z) \approx z \quad \text{for } x \rightarrow \pm\infty, \quad (4a)$$

$$\text{Im}[w] = 0 \quad \text{at } y = 0, \quad (4b)$$

$$\text{Im}[w] = \pi \quad \text{at } y = \pi, \quad (4c)$$

$$\text{Re}[w] = 0 \quad \text{on } \partial D_t. \quad (4d)$$

From conditions (4b)-(4d) one concludes that the flow domain in w -plane corresponds to a horizontal strip $0 < \psi < \pi$, $-\infty < \phi < \infty$, with a vertical slit inside it representing the bubble boundary, $\partial D(t)$, as shown in Fig. 1(b).

Let us now introduce the function $W(\zeta, t)$ through the composition

$$W(\zeta, t) \equiv w(z(\zeta, t)). \quad (5)$$

The boundary conditions (4) for the complex potential $w(z, t)$ can now be recast in terms

of the function $W(\zeta, t)$ as

$$W(\zeta, t) \approx \mp \ln(\zeta \mp \zeta_{\pm}) \quad \text{for } \zeta \rightarrow \zeta_{\pm}, \quad (6a)$$

$$\text{Im}[W] = 0, \pi \quad \text{for } \zeta \in C_0^{\mp}, \quad (6b)$$

$$\text{Re}[W] = 0 \quad \text{for } \zeta \in C_1. \quad (6c)$$

Thus the mapping $w = W(\zeta, t)$ conformally takes the annulus D_{ζ} to the strip domain in the w -plane shown in Fig. 1(b).

The kinematic boundary condition, $\partial\phi/\partial n = V_n$, can also be written in terms of $W(\zeta, t)$. To this end, we first recall that

$$V_n = \mathbf{V} \cdot \mathbf{n} = \text{Im}[(\dot{x} - i\dot{y})z_s] = \text{Im}[\bar{z}_t z_s], \quad (7)$$

where $\mathbf{n} = (n_x, n_y)$ is the unit vector normal to the interface, s denotes arclength, and $z_s = n_x + in_y$. Similarly,

$$v_n = \text{Im}[(v_x - iv_y)z_s] = \text{Im}[w'(z)z_s] = \text{Im}\left[\frac{W_{\zeta}}{z_{\zeta}}z_s\right]. \quad (8)$$

Furthermore one can readily show that for $\zeta \in C_1$ we have

$$z_s = i \frac{\zeta z_{\zeta}}{\rho |z_{\zeta}|}. \quad (9)$$

Equating (7) and (8), and making use of (9), we obtain

$$\text{Re}[\zeta z_{\zeta} \bar{z}_t] = \text{Re}[\zeta W_{\zeta}], \quad \text{for } \zeta \in C_1. \quad (10)$$

This is a generalization of the so-called Polubarinova-Galin equation [47] for the case where the interface is the image of a circle of radius ρ centered at the origin and the flow is described by a generic complex potential $W(\zeta, t)$. (For the so-called injection problem in an unbounded cell, see, e.g., [47], the interior of the unit circle C_0 is mapped to the fluid region, with C_0 mapped to the interface and the origin mapped to infinity, and the fluid is removed by a sink at infinity, i.e., $W(\zeta) = -(Q/2\pi)\ln\zeta$, resulting in the well known Polubarinova-Galin equation $\text{Re}(\zeta z_{\zeta} \bar{z}_t) = -Q/2\pi$.)

C. The Schwarz function

The first three equations in (1) are known [47] to be equivalent to

$$\mathcal{S}_t = 2w_z, \quad (11)$$

where $\mathcal{S}(z, t)$ is the Schwarz function [48] of the interface ∂D_t , defined as $\bar{z} = \mathcal{S}(z, t)$ for $z \in \partial D_t$. In (11) subscripts denote partial derivatives. An important result follows from (11): *all singularities of $\mathcal{S}(z, t)$ in $D(t)$ that are different from those of $w(z)$ must be constants of motion* [47]. As will see below, this property is the key to the integrable structure of the problem of interface dynamics in a Hele-Show cell.

The Schwarz function of the interface ∂D_t has the following useful representation in the ζ -plane:

$$g(\zeta, t) \equiv \mathcal{S}(z(\zeta, t), t) = \bar{z}(\rho^2/\zeta, t). \quad (12)$$

where we used that $\bar{\zeta} = \rho^2/\zeta$ for $\zeta \in C_1$ and have introduced the notation $\bar{f}(\zeta) = \overline{f(\bar{\zeta})}$. Notice that (12) is valid for $\zeta \in C_1$ and elsewhere by analytic continuation.

III. EXACT SOLUTIONS

A. The complex potential

The complex potential, $W(\zeta, t)$, satisfying the boundary conditions (6) is given by

$$W(\zeta) = i\frac{\gamma}{2} + \log \frac{P(e^{-i\gamma}\zeta; \rho^2)P(\rho^2\zeta; \rho^2)}{P(\zeta; \rho^2)P(\rho^2e^{-i\gamma}\zeta; \rho^2)}, \quad (13)$$

where the function $P(\zeta; \rho)$ is defined by

$$P(\zeta; \rho) = (1 - \zeta) \prod_{m=1}^{+\infty} (1 - \rho^{2m}\zeta)(1 - \rho^{2m}/\zeta). \quad (14)$$

For later use we note that $P(\zeta; \rho)$ satisfies the following symmetry relations:

$$P(1/\zeta; \rho) = -\frac{1}{\zeta}P(\zeta; \rho), \quad (15)$$

$$P(\rho^2/\zeta; \rho) = P(\zeta; \rho), \quad (16)$$

from which we can derive another useful relation:

$$P(\rho/\zeta; \rho) = P(\rho\zeta; \rho). \quad (17)$$

It is easy to verify that $W(\zeta)$ satisfies the required boundary conditions on the circles C_0

and C_1 . For instance, for $\zeta \in C_0$ we obtain

$$\begin{aligned}
\overline{W(\zeta, t)} &= -i\frac{\gamma}{2} + \log \frac{P(e^{i\gamma}\bar{\zeta}; \rho^2)P(\rho^2\bar{\zeta}; \rho^2)}{P(\bar{\zeta}; \rho^2)P(\rho^2e^{i\gamma}\bar{\zeta}; \rho^2)} \\
&= -i\frac{\gamma}{2} + \log \frac{P(e^{i\gamma}/\zeta; \rho^2)P(\rho^2/\zeta; \rho^2)}{P(1/\zeta; \rho^2)P(\rho^2e^{i\gamma}/\zeta; \rho^2)} \\
&= -i\frac{\gamma}{2} + \log \frac{e^{i\gamma}P(e^{-i\gamma}\zeta; \rho^2)P(\rho^2\zeta; \rho^2)}{P(\zeta; \rho^2)P(\rho^2e^{-i\gamma}\zeta; \rho^2)} \\
&= W(\zeta, t),
\end{aligned}$$

where in the second passage we used that $\bar{\zeta} = 1/\zeta$, for $\zeta \in C_0$, and in the third equality use was made of relations (15) and (17). Here we have chosen the branch of the logarithmic function in (13) such that $\text{Im}[W] = 0$ on the lower segment C_0^- of the unit circle C_0 , which implies in turn that $\text{Im}[W] = \pi$ for $\zeta \in C_0^+$. We have thus verified condition (6b).

Similarly, taking the complex conjugate of (13) for $\zeta \in C_1$ and using that $\bar{\zeta} = \rho^2/\zeta$ for $\zeta \in C_1$, one finds

$$\begin{aligned}
\overline{W(\zeta, t)} &= -i\frac{\gamma}{2} + \log \frac{P(\rho^2e^{i\gamma}/\zeta; \rho^2)P(\rho^4/\zeta; \rho^2)}{P(\rho^2/\zeta; \rho^2)P(\rho^4e^{i\gamma}/\zeta; \rho^2)} \\
&= -i\frac{\gamma}{2} + \log \frac{P(\rho^2e^{-i\gamma}\zeta; \rho^2)P(\zeta; \rho^2)}{P(\rho^2\zeta; \rho^2)P(\zeta; \rho^2)} \\
&= -W(\zeta, t),
\end{aligned}$$

where we used (16) and (17) in the second passage. Hence $\text{Re}[W] = 0$ for $\zeta \in C_1$, as required.

B. The conformal mapping

Here we shall deal exclusively with solutions that remain *non-singular* for all times, in which case the singularities of the mapping $z(\zeta, t)$ must all be logarithmic branch points [39, 40]. Other possible type of solutions, such as polynomial or rational functions, are not physically acceptable, as they would inevitably develop singularities (e.g., cusps) in finite time.

In view of the preceding discussion, we shall consider the following general solution for the conformal mapping $z(\zeta, t)$ describing the bubble dynamics:

$$\begin{aligned}
z(\zeta, t) &= d(t) + i\Delta + \log \frac{P(e^{-i\gamma}\zeta; \rho^2)}{P(\zeta; \rho^2)} + \alpha_0 \log \frac{P(e^{-i\gamma}\zeta/\rho^2; \rho^2)}{P(\zeta/\rho^2; \rho^2)} + \\
&\quad + \sum_{k=1}^N \{ \alpha_k \log P(a_k/\zeta; \rho^2) + \bar{\alpha}_k \log P(\bar{a}_k\zeta; \rho^2) \}, \tag{18}
\end{aligned}$$

where $d(t)$ is real, $a_k(t) \notin D_\zeta$, $k = 1, \dots, N$, are complex time-dependent parameters, α_0 is a real constant with $|\alpha_0| \leq 1$, α_k , $k = 1, \dots, N$, are complex constants, and Δ is a real quantity given by

$$\Delta = \frac{\gamma}{2}(1 + 2\alpha_0). \quad (19)$$

We must also have

$$\operatorname{Re} \sum_{k=1}^N \alpha_k = 0, \quad (20)$$

to ensure univalence of the map (18). For reasons to be explained later, the initial values of $a_k(0)$ are restricted to be inside the circle C_1 and outside the circle obtained by the inversion of C_0 in C_1 , i.e., $\rho^2 < |a_k(0)| < \rho$. (We remark parenthetically that the term containing α_0 in (18) was not explicitly considered in [40].)

Using the properties of the function $P(\zeta; \rho)$ given above we can verify that the mapping function (18) satisfies the required boundary condition on C_0 , namely $\operatorname{Im}[z(\zeta, t)] = \text{const.}$. To see this, first take the complex conjugate of (18) for $\zeta \in C_0$:

$$\begin{aligned} \overline{z(\zeta, t)} &= d(t) - i\Delta + \log \frac{P(e^{i\gamma}/\zeta; \rho^2)}{P(1/\zeta; \rho^2)} + \alpha_0 \log \frac{P(e^{i\gamma}/\zeta \rho^2; \rho^2)}{P(1/\zeta \rho^2; \rho^2)} + \\ &\quad + \sum_{k=1}^N \{ \bar{\alpha}_k \log P(\bar{a}_k \zeta; \rho^2) + \alpha_k \log P(a_k/\zeta; \rho^2) \} \\ &= d(t) - i\Delta + \log \frac{e^{i\gamma} P(e^{-i\gamma} \zeta; \rho^2)}{P(\zeta; \rho^2)} + \alpha_0 \log \frac{e^{i2\gamma} P(e^{-i\gamma} \zeta / \rho^2; \rho^2)}{P(\zeta / \rho^2; \rho^2)} + \\ &\quad + \sum_{k=1}^N \{ \alpha_k \log P(a_k/\zeta; \rho^2) + \bar{\alpha}_k \log P(\bar{a}_k \zeta; \rho^2) \}, \end{aligned} \quad (21)$$

where in the second passage we used (15) and (17). After some simplification, the previous equation becomes

$$\begin{aligned} \overline{z(\zeta, t)} &= d(t) + i\Delta + \log \frac{P(e^{-i\gamma} \zeta; \rho^2)}{P(\zeta; \rho^2)} + \alpha_0 \log \frac{P(e^{-i\gamma} \zeta / \rho^2; \rho^2)}{P(\zeta / \rho^2; \rho^2)} \\ &\quad + \sum_{k=1}^N \{ \alpha_k \log P(a_k/\zeta; \rho^2) + \bar{\alpha}_k \log P(\bar{a}_k \zeta; \rho^2) \} = z(\zeta, t), \end{aligned} \quad (22)$$

which proves that $\operatorname{Im}[z(\zeta, t)] = 0$ for $\zeta \in C_0^-$ and $\operatorname{Im}[z(\zeta, t)] = \pi$ for $\zeta \in C_0^+$, as desired. (Here again a suitable choice of the branch of the log function was made.)

C. The Schwarz function and its singularities

Let us now compute the Schwarz function $g(\zeta, t)$. Taking the complex conjugate of (18) for $\zeta \in C_1$ and using that $\bar{\zeta} = \rho^2/\zeta$ for $\zeta \in C_1$, we obtain

$$g(\zeta, t) = d(t) - i\Delta + \log \frac{P(\rho^2 e^{i\gamma}/\zeta; \rho^2)}{P(\rho^2/\zeta; \rho^2)} + \alpha_0 \log \frac{P(e^{i\gamma}/\zeta; \rho^2)}{P(1/\zeta; \rho^2)} + \sum_{k=1}^N \{ \bar{\alpha}_k \log P(\bar{\alpha}_k \zeta / \rho^2; \rho^2) + \alpha_k \log P(\rho^2 a_k / \zeta; \rho^2) \}, \quad (23)$$

which upon using (15) yields

$$g(\zeta, t) = d(t) + i\frac{\gamma}{2} + \log \frac{P(e^{-i\gamma}\zeta/\rho^2; \rho^2)}{P(\zeta/\rho^2; \rho^2)} + \alpha_0 \log \frac{P(e^{-i\gamma}\zeta; \rho^2)}{P(\zeta; \rho^2)} + \sum_{k=1}^N \{ \alpha_k \log P(\rho^2 a_k / \zeta; \rho^2) + \bar{\alpha}_k \log P(\bar{\alpha}_k \zeta / \rho^2; \rho^2) \}. \quad (24)$$

We shall next determine the location of the singularities of $g(\zeta, t)$ in the circular domain D_ζ , from which we can conclude about the presence of singularities of $S(z, t)$ in the fluid domain $D(t)$. As we will see below, $S(z, t)$ has logarithmic singularities at N finite points in $D(t)$ and, if $\alpha_0 \neq 0$, also a simple pole at infinity.

1. Finite singularities

As mentioned before, the singularities a_k are initially placed within the region $\rho^2 < |a_k| < \rho$, which implies from (24) that the only singularities of $g(\zeta, t)$ in the extended domain F_0 are the points $\zeta_k = \rho^2/\bar{a}_k$ and $\varphi_0(\zeta_k) = a_k/\rho^2$, for $k = 1, \dots, N$. We thus conclude that the only singularities of $S(z, t)$ in the extended fluid domain $D(t) \cup \overline{D(t)}$ are located at the points β_k and $\bar{\beta}_k$, where $\beta_k = z(\rho^2/\bar{a}_k, t)$, which

$$\beta_k = d(t) + i\frac{\gamma}{2} + \log \frac{P(e^{-i\gamma}\rho^2/\bar{a}_k; \rho^2)}{P(\rho^2/\bar{a}_k; \rho^2)} + \alpha_0 \log \frac{P(e^{i\gamma}\bar{a}_k; \rho^2)}{P(\bar{a}_k; \rho^2)} + \sum_{m=1}^N \{ \alpha_m \log P(a_m \bar{a}_k / \rho^2; \rho^2) + \bar{\alpha}_m \log P(\rho^2 \bar{a}_m / \bar{a}_k; \rho^2) \}, \quad (25)$$

Since the β_k 's are singular points of $S(z, t)$ in the fluid region but where the flow is regular, these points must remain fixed in time:

$$\dot{\beta}_k = 0, \quad (26)$$

where dot denotes time derivative.

Alternatively, the conserved quantities β_k can be obtained by inserting (13) and (18) into (10) and cancelling out the divergent terms on $\zeta_k = \rho^2/\bar{a}_k$ that appear on the left-hand side of this equation (and which are not present on the corresponding right-hand side).

2. Singularity at infinity

It also follows from (24) that if $\alpha_0 \neq 0$, then $g(\zeta, t)$ is singular at the points $\zeta_+ = 1$ and $\zeta_- = e^{i\gamma}$, which implies that $S(z, t)$ has singularities at $x = \pm\infty$. If, on the contrary, $\alpha_0 = 0$ then $S(z, t)$ is *regular* at infinity. One can use the behavior of $S(z, t)$ at infinity to obtain two extra conserved quantities.

First note that multiplying (24) by α_0 , subtracting the result from (18), and then taking the limit $\zeta \rightarrow \zeta_{\pm}$, one finds that

$$g(\zeta, t) - \alpha_0 z(\zeta, t) \approx (1 - \alpha_0)d(t) + C_{\pm}, \quad (27)$$

where

$$\begin{aligned} C_{\pm} = & i\frac{\gamma}{2}(1 - \alpha_0 - 2\alpha_0^2) + (1 - \alpha_0^2) \log \frac{P(e^{-i\gamma}\zeta_{\pm}; \rho^2)}{P(\zeta_{\pm}; \rho^2)} \\ & + \sum_{k=1}^N \{ \alpha_k \log P(\rho^2 a_k / \zeta_{\pm}; \rho^2) + \bar{\alpha}_k \log P(\bar{a}_k \zeta_{\pm} / \rho^2; \rho^2) \} \\ & - \alpha_0 \sum_{k=1}^N \{ \alpha_k \log P(a_k / \zeta_{\pm}; \rho^2) + \bar{\alpha}_k \log P(\bar{a}_k \zeta_{\pm}; \rho^2) \}. \end{aligned}$$

Furthermore one can show that

$$\text{Im}[C_{\pm}] = -\frac{\gamma}{2}\alpha_0(1 + \alpha_0) - \text{Im} \sum_k \alpha_k \log a_k \quad (28)$$

Equation (27) implies that the Schwarz function $S(z, t)$ has a simple pole at infinity:

$$S(z, t) \approx \alpha_0 z + (1 - \alpha_0)d(t) + C_{\pm}(t), \quad \text{for } x \rightarrow \pm\infty. \quad (29)$$

Now inserting (29) into (11) and noting that $w_z \approx 1$ for $|z| \rightarrow \infty$, we then conclude that

$$(1 - \alpha_0)\dot{d} + \dot{C}_{\pm} = 2$$

thus implying that the quantities β_{\pm} defined by

$$\beta_{\pm} = (1 - \alpha_0)d(t) + C_{\pm} - 2t \quad (30)$$

are constants of motion:

$$\dot{\beta}_{\pm} = 0. \quad (31)$$

(Alternatively, the conserved quantities β_{\pm} can be obtained by inserting (13) and (18) into (10) and matching the divergent terms for $\zeta \rightarrow \zeta_{\pm}$ that appear on both sides of this equation.) It follows from (28) and (30) that $\text{Im}[\beta_{+}] = \text{Im}[\beta_{-}]$, hence there are only three independent real parameters between the two complex constants β_{\pm} .

Note that there are $2N + 3$ conserved real quantities, corresponding to N complex quantities β_k and three conserved real quantities from β_{\pm} (recalling that $\text{Im}[\beta_{+}] = \text{Im}[\beta_{-}]$), where the values of the β_k 's and β_{\pm} are determined by the initial conditions and remain constant in time. Correspondingly, there are $2N + 3$ real time-dependent parameters to solve for, namely N complex quantities $a_k(t)$ and three real parameters, $d(t)$, $\gamma(t)$ and $\rho(t)$. Thus, equations (26) and (31) provide the complete time-dependence of the mapping parameters $a_k(t)$, $\zeta_{\pm}(t)$, and $d(t)$. Numerically solving these equation for subsequent times, allows us to obtain the time evolution of the bubble until it reaches the steady regime. A detailed numerical analysis of the solutions above is reported in Sec. IV, but before let us discuss the steady regime.

D. Long-time asymptotic regime.

Let us now investigate the steady regime of the exact solutions above in the limit of $t \rightarrow \infty$. First, note from (30) that in order to keep β_{\pm} constant for all times, given that C_{\pm} remains finite, the parameter $d(t)$ must behave as

$$d(t) = Ut \quad \text{for} \quad t \rightarrow \infty, \quad (32)$$

where

$$U = \frac{2}{1 - \alpha_0}. \quad (33)$$

This ensures that the divergence of the term $2t$ in (30) is canceled off for $t \rightarrow \infty$. We shall see shortly that the parameter U defined above is precisely the bubble asymptotic speed in the steady regime.

Similarly, using (32) in (25), one sees that another term in the right-hand side of (25) must diverge for $t \rightarrow \infty$ as to cancel the divergence of $d(t)$, thus ensuring that β_k remains

constant for all times. Inspection of (25) reveals that the only such possibility is if the point ρ^2/\bar{a}_k (which is the reflection of a_k in the inner circle of radius ρ) approaches the source at $e^{i\gamma}$. We thus conclude that all a_k 's must behave asymptotically as

$$a_k = \rho^2 e^{i\gamma} \quad \text{for} \quad t \rightarrow \infty. \quad (34)$$

If we now insert (32) and (34) into (18), and use that $\sum_{k=1}^N \text{Re}[\alpha_k] = 0$, we obtain that for $t \rightarrow \infty$ the solution becomes

$$z(\zeta, t) = Ut + i\Delta + \log \frac{P(e^{-i\gamma}\zeta; \rho^2)}{P(\zeta; \rho^2)} + \left(1 - \frac{2}{U}\right) \log \frac{P(e^{-i\gamma}\zeta/\rho^2; \rho^2)}{P(\zeta/\rho^2; \rho^2)}. \quad (35)$$

This is precisely the one-parameter family of solutions reported in Refs. [35, 49] for an asymmetric bubble steadily moving in a Hele-Shaw cell, which itself is a generalization of the symmetric bubble originally obtained by Taylor and Saffman [2]. In the next section we show some examples of bubble evolution described by the solutions (18).

IV. NUMERICAL EXAMPLES

As already discussed, equations (25) and (30) provide the complete time-dependence of the parameters $a_k(t)$, $\gamma(t)$, $\rho(t)$, and $d(t)$, once their initial values are given. More explicitly, if we write $a_k(t) = \xi_k(t) + i\eta_k(t)$, we can use Eqs. (26) and (31) to obtain a set of $2N + 3$ ordinary differential equations for equal number of real-valued parameters: d , γ , ρ , and $\{\xi_k, \eta_k | k = 1, \dots, n\}$. By integrating these equations numerically, it is then possible to compute the time evolution of the interface. Initial conditions should however be chosen carefully, since some of them may lead to finite-time ‘blow-up’ because of loss of univalence of the mapping $z(\zeta, t)$. Below we show several examples of bubble evolutions described by our solutions, both for the case where the solutions exist for all times and for situations when there occurs bubble ‘breakup,’ in the sense that the interface self-intersects at some finite time.

A. Solutions with a steady state

We have seen in Sec. III D that if a solution exists for all times, then the bubble will necessarily reach a steady regime where it moves with a constant speed U and without

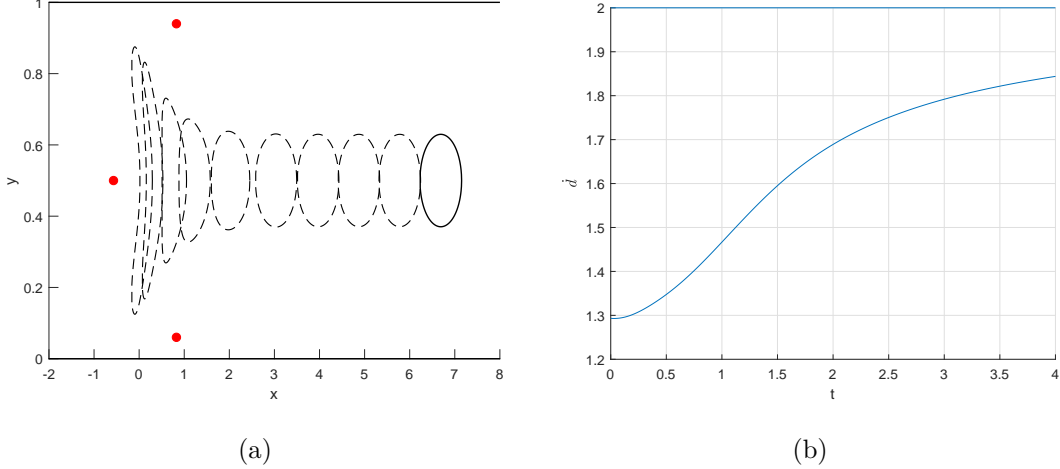


Figure 2: (a) Bubble evolution leading to a symmetric steady shape with $U = 2$. The initial shape corresponds to Eq. (18) with the parameters $\gamma = \pi$, $\alpha_1 = -0.4$, $\alpha_2 = \alpha_3 = 0.2$, $a_1(0) = -0.3$, $a_2(0) = \overline{a_3(0)} = 0.15 + 0.1i$, and $\rho(0) =$. Successive shapes are shown at the time instants $t = 0, 0.1724, 0.5228, 0.8340, 1.3011, 1.8275, 2.2960, 2.7487, 3.2021, 3.6570$. The red dots indicate the location of the singularities β_k , $k = 1, 2, 3$, of the Schwarz function. (b) The time derivative of the parameter $d(t)$ plotted as a function of time.

changing its shape. The value of the asymptotic velocity U is determined via (33) by the parameter α_0 , which corresponds to the strength of the logarithmic singularity of the mapping $z(\zeta, t)$ at the special points $a_0^+ = \rho^2$ and $a_0^- = \rho^2 e^{i\gamma}$; see (18). Alternatively, α_0 can be seen as the strength (residue) of the simple pole of the Schwarz function $S(z, t)$ at infinity; see (29).

Let us first consider solutions when the bubble attains the asymptotic velocity $U = 2$, which occurs whenever $\alpha_0 = 0$. In Fig. 2 we show an example of this case for a symmetric initial condition corresponding to the following parameters: $\gamma = \pi$, $\alpha_1 = 0.2$, $\alpha_2 = -0.4$, $\alpha_3 = 0.2$, $a_1(0) = -0.3$, $a_2(0) = 0.15 + 0.1i = \overline{a_3(0)}$, and $\rho(0) =$. In Fig. 2(a) we display successive plots of the bubble interface at several times. The red dots in this figure indicate the location of the fixed singularities β_k , $k = 1, 2, 3$, of the Schwarz function $S(z, t)$. In Fig. 2(b) we plot the quantity \dot{d} as a function of time, which gives an estimate of the bubble velocity since we have $d(t) \rightarrow Ut$ as $t \rightarrow \infty$. Comparing Figs. 2(a) and 2(b), one sees that the interface moves slowly at first (i.e., $\dot{d}(0) \approx 1.3 < U = 2$), but once it gets past the two singularities of $S(z, t)$ that are initially upstream of the bubble, it quickly speeds up toward the asymptotic velocity $U = 2$.

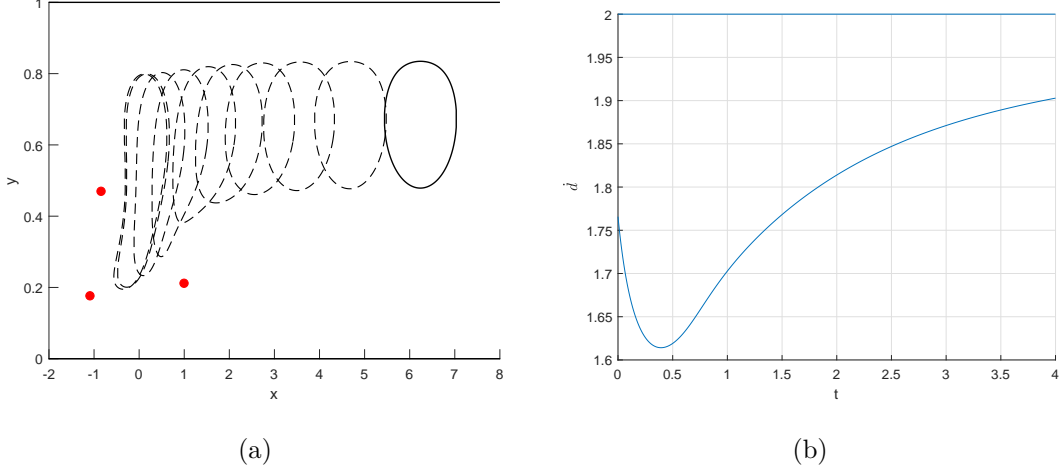


Figure 3: (a) Bubble evolution leading to a non-symmetric steady shape with $U = 2$. Here the parameters are $\alpha_0 = 0$, $\alpha_1 = -0.4$, $\alpha_2 = \alpha_3 = 0.2$, $a_1(0) = -0.3$, $\gamma(0) = \pi$, $a_2(0) = -0.2 - 0.1i$, $a_3(0) = 0.2 - 0.1i$, and $\rho(0) =$. The bubble shapes are shown for the times $t = 0, 0.0343, 0.2373, 0.5241, 0.8454, 1.1490, 1.5136, 1.9591, 2.5337, 3.3132$. (b) The time derivative of the parameter $d(t)$ plotted as a function of time.

In Fig. 3 we show an example of a bubble evolution where the initial shape is non-symmetric, leading therefore to an asymmetric steady shape. Here the parameters are $\alpha_0 = 0$, $\alpha_1 = -0.4$, $\alpha_2 = \alpha_3 = 0.2$, $a_1(0) = -0.3$, $\gamma(0) = \pi$, $a_2(0) = -0.2 - 0.1i$, $a_3(0) = 0.2 - 0.1i$, and $\rho(0) =$. In Fig. 3(a) successive interface shapes are shown, with the red dots again indicating the location of the fixed singularities of $S(z, t)$, while Fig. 3(b) shows the plot of $\dot{d}(t)$. It is interesting to see the effect of the singularities of $S(z, t)$ on the bubble evolution. Notice that as the bubble approaches the singularity furthest ahead, the interface slows down and deforms considerably. Eventually, however, the bubble succeeds to pass this last singularity, after which it is ‘free’ to speed up towards $U = 2$, quickly reaching a (nearly) steady shape.

As discussed above, solutions leading to an asymptotic velocity $U \neq 2$ are obtained by choosing $\alpha_0 \neq 0$ in (18), where the speed U is related to α_0 via (33). In Fig. 4(a) we show a case where the final speed is $U = 1.5$, whereas for the bubble evolution shown in Fig. 4(a) the bubble reaches the asymptotic velocity $U = 2.5$. Note that bubbles that move with velocity $U < 2$ become compressed in the flow direction and elongated in the transversal direction, whereas for bubbles with $U > 2$ the opposite happens, as expected [17].

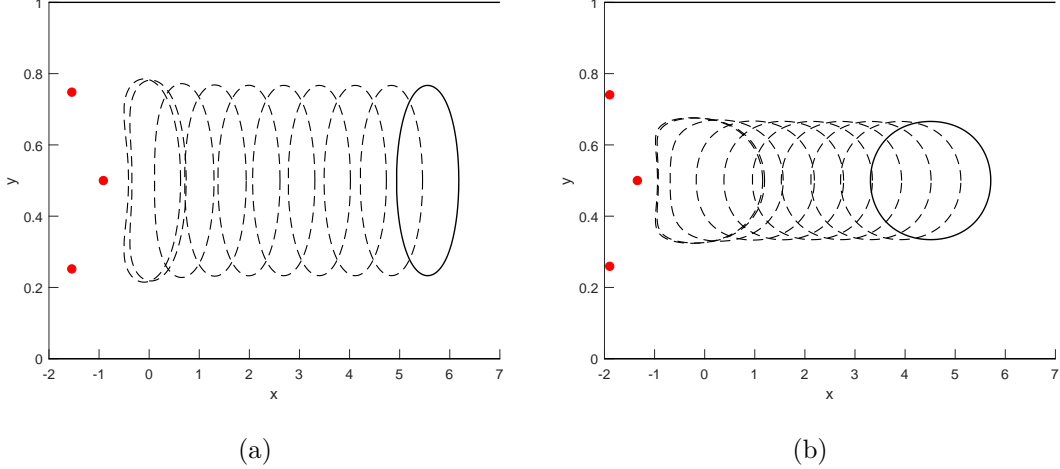


Figure 4: (a) Bubble evolution for an initial shape leading to an asymptotic velocity $U = 1.5$. The parameters are (a): $\alpha_0 = -0.33$, $\alpha_1 = 0.2$, $\alpha_2 = -0.4$, $\alpha_3 = 0.2$, $a_1(0) = -0.2 - 0.05i$, $a_2(0) = -0.3$, $a_3(0) = -0.2 + 0.05i$. (b) Bubble evolution leading to $U = 2.5$. Here the parameters are (a): $\alpha_0 = 0.2$, $\alpha_1 = 0.2$, $\alpha_2 = -0.4$, $\alpha_3 = 0.2$, $a_1(0) = -0.2 - 0.05i$, $a_2(0) = -0.3$, $a_3(0) = -0.2 + 0.05i$.

B. Bubble ‘breakup’

Depending on the initial condition, it may so happen that the bubble does *not* successfully manage to get past the singularities of $S(z, t)$, leading to a blow up of the solution in finite time, in the sense that the solution cannot be continued past the time when the mapping $z(\zeta, t)$ ceases to be univalent, i.e., the interface self-intersects. After such a ‘breakup’ point the solution is no longer physically valid.

Bubble breakup will always occur, for example, if we start with a symmetric shape having a singularity of $S(z, t)$ located at a point ahead of the bubble on the channel centerline. In such a situation, because of the symmetry, there is no way that the interface can pass the singularity, thus implying that at some point in time the interface must necessarily intersect itself. An example of this situation is displayed in Fig. 5(a). One clearly sees in this figure that, as the bubble approaches the singularity (red dot) of $S(z, t)$, the center part of the fore side of the interface gets ‘pinned down’ by the singularity, while both sides of the fore-interface tend to go round the singularity, so that an incipient ‘fjord’ develops. However, as the aft-interface continues to advance, it will eventually ‘touch’ the point of the fore interface that remains stuck. The last interface shown in Fig. 5(a) corresponds to shortly before this touching point. Physically the touching of the two sides of the interface would result in

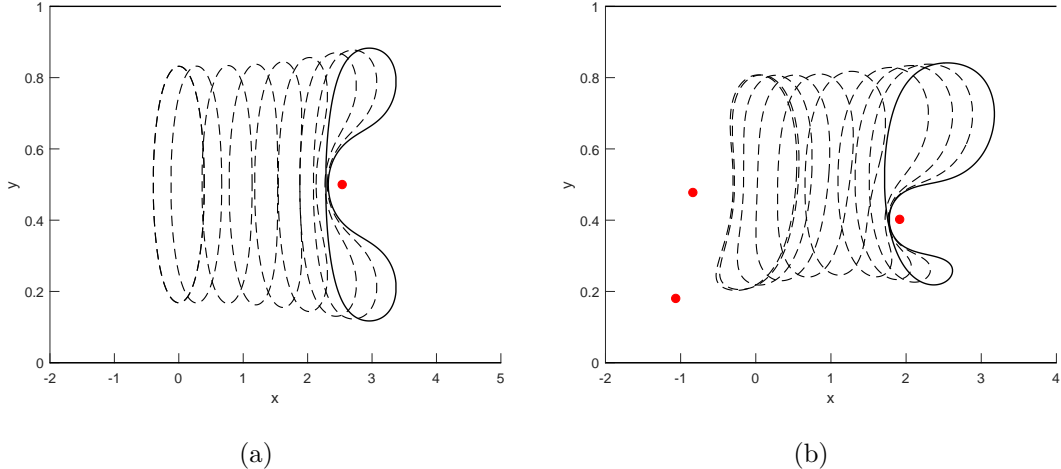


Figure 5: Time evolution of symmetric (a) and non-symmetric (b) bubbles, showing ‘beakup’ at finite time. The parameters are (a): $\alpha_0 = 0$, $\alpha_1 = -0.3$, $\alpha_2 = 0.3$, $a_1(0) = -0.17$, $a_2(0) = 0.18$; and (b): $\alpha_0 = 0$, $\alpha_1 = 0.2$, $\alpha_2 = -0.4$, $\alpha_3 = 0.2$, $a_1(0) = -0.2 - 0.1i$, $a_2(0) = -0.3$, $a_3(0) = 0.2 - 0.015i$

the bubble breaking up into two smaller identical bubbles. Mathematically, our solutions are not valid past the ‘breakup’ point because the conformal mapping $z(\zeta, t)$ is no longer univalent.

Asymmetric bubble breakup can also occur, as shown in Fig. 5(b). In this figure, the initial shape is not symmetric and the singularity of $S(z, t)$ that induces the breakup ends up closer to the bottom part of the interface. Hence the incipient fjord does not form symmetrically along the channel centreline, as was the case in Fig. 5(a), so that now the bubble would (in a real situation) pinch off into a smaller and a larger bubble.

V. VELOCITY SELECTION

As already mentioned in the introduction, the so-called *selection problem* for Hele-Shaw flows concerns the fact that out of the continuous family of analytical solutions for a steadily moving finger [1] or bubble [2] only a specific pattern (namely, that with velocity $U = 2$) is experimentally observed in the limit that surface tension effects become vanishingly small. In the mid 1980s, it was shown by several groups [33] that the inclusion of small surface tension effects can select the observed pattern. Subsequent evidence showed however that surface tension is not the only mechanism that can lead to pattern selection, as the kinetic undercooling boundary condition also produces the same selection scenario [36, 37]. In

fact, similar pattern selection has been observed even in non-fluid systems, such as in the propagation of streamers (finger-like ionization fronts) in electric breakdown [9], where there is no analog of surface tension. Taken together, these results suggest that the selection mechanism in Hele-Shaw flows is not specifically dependent upon the boundary condition one chooses to regularize the idealized problem.

Indeed, it has been shown [39] that the velocity selection for a finger can be obtained entirely within the context of exact time-dependent solutions *without surface tension*, as the selected pattern (with $U = 2$) is the only stable attractor of the dynamics. More recently, it has been argued that a similar dynamical selection mechanism also holds for Hele-Shaw bubbles [40–42]. In what follows we give a more complete demonstration of the argument, briefly discussed in Ref. [40], that solves the selection problem for a bubble through the stability analysis of time-dependent solutions of the sort described in Sec. III.

First recall that a special aspect of the steady solutions with $U \neq 2$ is that the mapping $z(\zeta, t)$ given in (35) has singularities at two fixed points, namely $a_0^+ = \rho^2$ and $a_0^- = \rho^2 e^{i\gamma}$, in the non-physical domain in the ζ plane. Suppose now that we perturb this steady solution slightly by causing an infinitesimal displacement of the singularities from the fixed points. More precisely, we consider an initial perturbed shape of the form

$$z(\zeta, 0) = d(0) + i\frac{\gamma}{2} + \log \frac{P(e^{-i\gamma}\zeta; \rho^2)}{P(\zeta; \rho^2)} + \frac{\alpha_0}{2} \log \frac{P(\zeta/(\rho^2 e^{i\gamma} + \varepsilon_-))P(1/\zeta(\rho^2 e^{-i\gamma} + \bar{\varepsilon}_-))}{P(\zeta/(\rho^2 + \varepsilon_+))P(1/\zeta(\rho^2 + \bar{\varepsilon}_+))}, \quad (36)$$

where $\alpha_0 = (1 - 2U^{-1})$ and $\varepsilon_{\pm}(0)$ are some small perturbations, i.e., $|\varepsilon_{\pm}(0)| \ll 1$. The form of the perturbed term above, i.e., last term in (36), is dictated by the requirement that it must have constant imaginary part on C_0 , so as to preserve the boundary condition $\text{Im}[z(\zeta, t)] = \text{const.}$, for $\zeta \in C_0$. One can also easily verify that Eq. (36) recovers the corresponding unperturbed solution (35) for $\varepsilon_{\pm} \rightarrow 0$. [To show this, use property (17) which implies that $P(1/\zeta \rho^2 e^{-i\gamma})/P(1/\zeta \rho^2) = e^{i2\gamma} P(e^{-i\gamma}\zeta/\rho^2)/P(\zeta/\rho^2)$.]

Since the perturbed mapping (36) now has singularities at the points $a_1 = \rho^2 e^{i\gamma} + \varepsilon_-$ and $a_2 = \rho^2 + \bar{\varepsilon}_+$, which no longer coincide with the fixed points, they must both approach the point $\rho^2 e^{i\gamma}$ as $t \rightarrow +\infty$, as shown in Sec. III D. In other words, $\varepsilon_-(t) \rightarrow 0$ and $\varepsilon_+(t) \rightarrow \rho^2(e^{i\gamma} - 1)$ for $t \rightarrow \infty$, thus cancelling the perturbation term in (36), so that in the steady

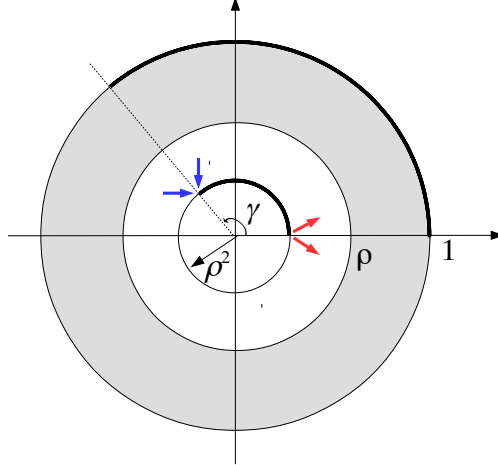


Figure 6: Schematic flow of the singularities $a_k(t)$ near the fixed points ρ^2 (repeller) and $\rho^2 e^{i\gamma}$ (attractor).

regime the solution becomes simply

$$z(\zeta, t) = 2t + i\frac{\gamma}{2} + \log \frac{P(e^{-i\gamma}\zeta; \rho^2)}{P(\zeta; \rho^2)}, \quad (37)$$

which corresponds precisely to a steady solution with velocity $U = 2$. This result, together with the discussion in Sec. IIID, demonstrates that the only *attractor* (i.e., stable fixed point) of the dynamical system $\{a_k(t)\}$ in the ζ -plane is the point $\rho^2 e^{i\gamma}$, whereas the point ρ^2 is a *repeller* (i.e., unstable fixed point) of the dynamics; a schematic of the flow of the singularities $a_k(t)$ near the fixed points $\rho^2 e^{i\gamma}$ and ρ^2 is shown in Fig. 6.

It is instructive to analyze the singularity dynamics as viewed from the physical z -plane. First note that the perturbation enacted by (36) has effectively split the pole at infinity of the Schwarz function $S(z, t)$ of the steady solution (35), see (29), into two logarithmic singularities that are at finite (albeit faraway) points, one being ahead and the other behind the bubble. Given that the singularities of $S(z, t)$ remain fixed in time in the z -plane, the bubble will eventually pass the singularity that lies ahead (since we assume that the solution exists for all times). As the bubble leaves all singularities of $S(z, t)$ infinitely far behind for $t \rightarrow \infty$ (and their net strength is null), the bubble will assume the asymptotic shape (37) whose Schwarz function is regular in the fluid domain.

In Fig. 7 we show an example of such a perturbation where a symmetric steady shape with $U = 4$ (and $\gamma = \pi$) was perturbed by slightly displacing the singularities from the fixed point $\pm\rho^2$. In this figure, the extra singularities of the Schwarz function that now appear

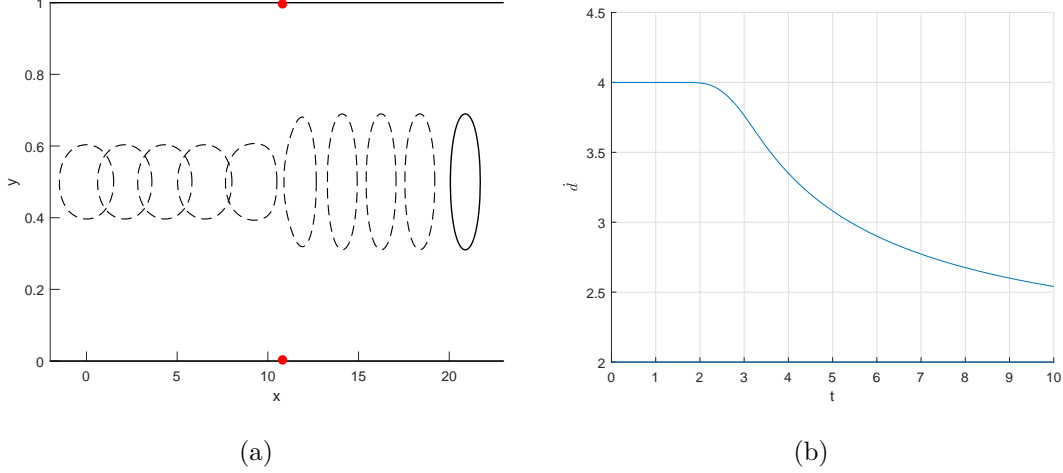


Figure 7: Shape evolution (a) and velocity (b) after perturbing a steady solution with $U = 4$. Here the initial shape corresponds to Eq. (36) with parameters $\alpha_0 = 0$, $\alpha_1 = 0.25$, $\alpha_2 = -0.125$, $\alpha_3 = -0.125$, $a_1(0) = -0.16 - 10^{-4}$, $a_2(0) = 0.16 + 10^{-7} + 10^{-5}i$, $a_3(0) = 0.16 + 10^{-7} - 10^{-5}i$. Time instant shown are $t = 0, 0.5274, 1.0793, 1.6306, 2.2904, 3.2246, 4.3490, 5.4190, 6.4867, 7.7407$.

ahead of the bubble are indicated by the red dots. One clearly sees in this figure that at first the bubble hardly feels the presence of these new singularities as it initially moves almost without deformation and with the same velocity $U = 4$ as the unperturbed steady shape. However, after the bubble passes the singularities of the Schwarz function at around $t \approx 2$, it suddenly expands in the transversal direction, thus reducing its speed towards the selected velocity $U = 2$.

The preceding analysis can be easily generalized to show that any perturbation of an initial shape that would otherwise yield $U \neq 2$ will instead lead to $U = 2$, so long as the singularities originally placed at ρ^2 and $\rho^2 e^{i\gamma}$ are displaced ever so slightly from the fixed points (meaning that the singularity of $S(z, 0)$ is ‘displaced’ from infinity). An example of this situation is shown in Fig. 8(a), where we compare the subsequent evolutions starting from two distinct but very similar initial shapes. In one case (black dashed lines) we start with an initial shape whose mapping $z(\zeta, 0)$ has singularities at the fixed points ρ^2 and $\rho^2 e^{i\gamma}$ as shown in (18), with $\alpha_0 = 0.2$ so that $U = 5/3$ will be obtained in the steady state. Superimposed to these ‘unperturbed’ interfaces we also show the resulting evolution (blue solid lines) for the case when we displace the singularities at the fixed points by a very small amount, while maintaining all other mapping parameters identical to the unperturbed case. The red dot furthest ahead (near the bottom wall) indicates the new location of the

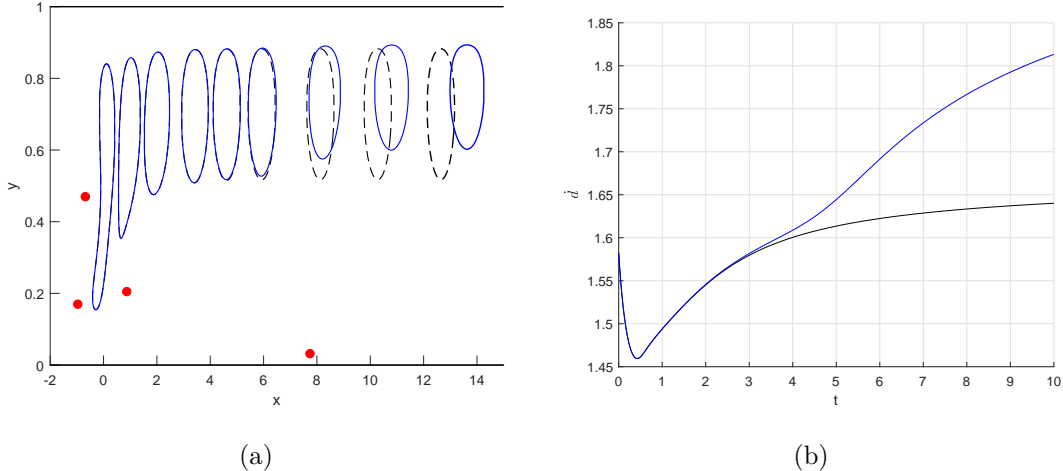


Figure 8: (a) Comparison between the evolution (black curves) starting with an initial shape leading to $U = 5/3$ and the evolution (blue curves) from a perturbed initial shape where the singularities of the mapping were slightly displaced from the fixed points; see text. The time instants are $t = 0, 0.6398, 1.3223, 2.2051, 2.9253, 3.7151, 5.0368, 6.3275, 7.7476$. (b) The bubble velocities, as measured by $\dot{d}(t)$, as a function of time for both cases shown in (a).

singularity of the Schwarz function that was originally at infinity (in the unperturbed case). As in Fig. 7, one sees that initially the perturbed interface essentially traces out the motion of the unperturbed evolution, but as soon as the bubble gets past the last singularity of $S(z, t)$ it quickly changes its shape and speed towards the selected pattern with $U = 2$, as can be seen in Fig. 8(b) where we plot the bubble velocity for both cases as a function of time.

The preceding stability argument thus shows that, even if we could prepare the (real) system with an initial condition corresponding to a steady solution with $U \neq 2$, inevitable perturbations will lead to a steady regime where the bubble moves with speed $U = 2$. In this context, surface tension is just one of many possible perturbations that can force the system toward the attractor, while also regularizing high curvatures.

VI. CONCLUSIONS

We have presented a general class of analytical solutions for the unsteady motion of a bubble in a Hele-Shaw channel. The solutions are given in terms of a conformal mapping from an annulus to the fluid region outside the bubble, with the corresponding mapping function

being written explicitly in terms of certain special (elliptic) functions. The time-dependent parameters that enter the solutions are given implicitly by a set of conservation laws which reflect the integrable nature of the Laplacian growth model. Numerically solving the set of ordinary differential equations that derives from these conservation laws allows us to follow the motion of the bubble in time for any given initial shape. Several examples of time-evolving bubbles have been presented. We have shown, both analytically and numerically, that in the asymptotic limit of large times, i.e., for $t \rightarrow \infty$, our time-dependent solutions approach the known steady solutions for a single bubble in a Hele-Shaw channel [2, 35, 40].

We have also shown that the steady solution with $U = 2V$ is the only stable attractor of the dynamics, whereas solutions with $U \neq 2V$ are the equivalent of an unstable fixed point (i.e., a repeller). The analysis reported here confirms in greater detail the argument, put forth in [39] for a finger and in [40] for a bubble, that surface tension is not necessary for velocity selection. In this scenario, the selection mechanism is encoded in the very dynamics of the Laplacian growth model (without any regularizing boundary condition), as the selected pattern is the only stable attractor of the dynamics. The dynamical selection mechanism for Hele-Shaw flows presented here is predicated on the asymptotic behavior of the Schwartz function for $|x| \rightarrow \infty$, and so it should apply whenever the point at infinity is in the fluid domain, such as in the case of a finite assembly of bubbles in either a channel or an unbounded cell.

Acknowledgments

This work was supported in part by the following Brazilian agencies: Conselho Nacional de Desenvolvimento Científico e Tecnológico (CNPq), under Grants 303772/2017-4 and 439299/2018-7, and Coordenação de Aperfeiçoamento de Pessoal de Nível Superior (CAPES).

-
- [1] P. G. Saffman and G. I. Taylor, Proc. R. Soc. Lond. A **245**, 312 (1958).
- [2] G. I. Taylor and P. G. Saffman, Q. J. Mech. Appl. Maths **12**, 265 (1959).
- [3] H. Lamb, *Hydrodynamics* (Cambridge University Press, Cambridge, 1906).
- [4] H. Darcy, *Les fontaines publiques de la ville de Dijon* (Dalmont, Paris, 1856).
- [5] S. Whitaker, Transp. Porous Med. **1**, 3 (1986).
- [6] J. S. Langer, Rev. Mod. Phys. **52**, 1 (1980).
- [7] A. P. Aldushin, B. J. Matkowsky, Combustion Sci. and Tech. **133**, 293 (1998).
- [8] M. Ben Amar, Physica D (Amsterdam, Neth.) **134**, 275 (1999).
- [9] A. Luque, F. Brau, and U. Ebert, Phys. Rev. E **78**, 016206 (2008).
- [10] J. Müller and W. van Saarloos, Phys. Rev. E **65**, 061111 (2002).
- [11] P. Pelcé, *Dynamics of Curved Fronts* (Academic Press, San Diego, 1988).
- [12] M. Mineev-Weinstein, P. B. Wiegmann, and A. Zabrodin, Phys. Rev. Lett. **84**, 5106 (2000).
- [13] I. Krichever, M. Mineev-Weinstein, P. Wiegmann, and A. Zabrodin, Physica D **198**, 1 (2004).
- [14] M. Mineev-Weinstein, M. Putinar, R. Teodorescu, J. Phys. A **41**, 263001 (2008).
- [15] O. Agam, E. Bettelheim, P. Wiegmann, and A. Zabrodin, Phys. Rev. Lett. **88**, 236801 (2002).
- [16] B. Gustafsson, R. Teodorescu, and A. Vasil'ev, *Classical and Stochastic Laplacian Growth* (Birkhäuser, Basel, 2014).
- [17] G. L. Vasconcelos, J. Fluid Mech. **780**, 299 (2015).
- [18] P. G. Saffman, Q. J. Mech. Appl. Maths **12**, 146–150 (1959).
- [19] S. D. Howison, J. Fluid Mech. **167**, 439–453 (1986).
- [20] M. Mineev-Weinstein and S. P. Dawson, Phys. Rev. E **50**, R24 (1994); Physica D **73**, 373 (1994).
- [21] D. Bensimon and P. Pelcé, Phys. Rev. A **33**, 4477–4478 (1986).
- [22] B. Shraiman and D. Bensimon, Phys. Rev. A **30**, 2840–2842 (1984).
- [23] S. Richardson, Eur. J. Appl. Math. **5**, 97–122 (1994).
- [24] S. Richardson, S. Phil. Trans. R. Soc. Lond. A **354**, 2513–2553 (1996).
- [25] M. C. Dallaston and S. W. McCue *Phys. Fluids* **24**, 052101 (2012).
- [26] D. G. Crowdy, Q. Appl. Math. **60**, 11–36 (2002).
- [27] J. S. Marshall, IMA J. App. Math. **81**, 723–749 (2016).

- [28] S. Richardson, *Eur. J. Appl. Math.* **12**, 571–599 (2001).
- [29] S. Richardson, *Eur. J. Appl. Math.* **7**, 345–366 (1996).
- [30] D. Crowdy and S. Tanveer, *J. Stat. Phys.* **114**, 1501–1536 (2004).
- [31] J. S. Marshall, *Q. Jl. Mech. Appl. Math.* **69**, 35–66 (2016).
- [32] J. S. Marshall, *Q. Jl. Mech. Appl. Math.* **69**, 1–33 (2016).
- [33] B. I. Shraiman, *Phys. Rev. Lett.* **56**, 2028 (1986); D. C. Hong and J. S. Langer, *ibid* **56**, 2032 (1986); R. Combescot, T. Dombre, V. Hakim, Y. Pomeau, and A. Pumir, *ibid* **56**, 2036 (1986); S. Tanveer, *Phys. Fluids* **30**, 1589 (1987).
- [34] S. Tanveer, *Phys. Fluids* **29**, 3537 (1986).
- [35] S. Tanveer, *Phys. Fluids* **30**, 651 (1987).
- [36] S. J. Chapman and J. R. King, *J. Eng. Math.* **46**, 1–32 (2003).
- [37] M. Dallaston and S. McCue, *ANZIAM J.* **52**, C124–C138 (2011).
- [38] C. C. Green, C. J. Lustri, and S. W. McCue, *Proc. R. Soc. A* **473** 20170050 (2017).
- [39] M. Mineev-Weinstein, *Phys. Rev. Lett.* **80**, 2113 (1998).
- [40] G. L. Vasconcelos and M. Mineev-Weinstein, *Phys. Rev. E* **89**, 061003(R) (2014).
- [41] A. H. Khalid, N. R. McDonald, and J. M. Vanden-Broeck, *Phys. Fluids* **27**, 012102 (2015).
- [42] M. Mineev-Weinstein and G. L. Vasconcelos, Velocity selection (without surface tension) in multi-connected Laplacian growth, arXiv:1501.01052 [physics.flu-dyn].
- [43] B. Shraiman and D. Bensimon, *Phys. Scr.* **T9**, 123–125 (1985);
- [44] W. Van Saarloos, *Phys. Rev. A* **37**, 211–229 (1988).
- [45] W. Van Saarloos, *Phys. Rep.* **386**, 29–222 (2003).
- [46] D. Burgess and S. Tanveer, *Phys. Fluids A* **3**, 367–379 (1991).
- [47] S. D. Howison, *Eur. J. Appl. Math.* **3**, 209 (1992).
- [48] P. J. Davis, *The Schwarz Function and its Applications*, Carus Mathematical Monograph No. 17 (The Mathematical Association of America, 1974).
- [49] G. L. Vasconcelos, *J. Fluid Mech.* **444**, 175 (2001).